Threshold krypton charge-state distributions coincident with *K*-shell fluorescence

G. B. Armen,[1] E. P. Kanter,[2] B. Krässig,[2] J. C. Levin,[1] S. H. Southworth,[2] and L. Young[2]
[1]*Department of Physics, University of Tennessee, Knoxville, Tennessee 37996*
[2]*Argonne National Laboratory, Argonne, Illinois 60439*

(Received 3 October 2002; revised manuscript received 7 January 2003; published 29 April 2003)

Measurements of Kr^{q+} yields in coincidence with *K*-shell fluorescence, as incident x-ray energy is varied across the *K*-shell threshold, are reported. Near threshold, we observe slight variations in the branching ratios as a function of energy, which are connected with the different behaviors of the flux-normalized partial yields for each *q*. The lower-*q* yields show a resonance peak near threshold superimposed on a smoothly rising edge, whereas the higher-*q* yields show only a smooth rise. A simple model is developed which accounts for these features, incorporating both the threshold photoexcitation and the cascade behavior of the spectator electrons.

DOI: 10.1103/PhysRevA.67.042718 PACS number(s): 32.80.Hd, 32.50.+d, 32.80.Fb

I. INTRODUCTION

When photoionized above an inner-shell threshold, atoms typically decay by either Auger-electron emission or x-ray fluorescence. Auger emission results in a doubly charged ion and two free electrons. X-ray fluorescence results in a singly charged ion with a free electron and photon. While it is often convenient to view these processes as decay of an intermediate inner-shell vacancy state, they are fundamentally a single-step resonant ionization phenomenon (see Ref. [1]). This distinction becomes important near threshold, where the two-step model of excitation followed by decay fails to describe the diagram [2,3] behavior. Furthermore, near threshold other states can also be produced in which the photoelectron is excited to a Rydberg (''spectator'') orbital rather than being ionized. In the radiative channel, this process is often referred to as Raman scattering, and results in a neutral atom and a photon. In the Auger channel, the result is a singly charged ion and one free electron. This process has been referred to as spectator Auger, resonant-Auger, and radiationless resonant-Raman scattering. This variety of names reflects the historical evolution, in our understanding, of the topic; each is still useful to some degree in emphasizing particular aspects of the various ways in which the process can be envisioned (see Ref. [4], and references therein).

Because these different states are distinguished by the charge of the residual ion, charge-state spectroscopy measured in coincidence with one of the ejected particles provides a powerful tool for studying various aspects of threshold physics. For example, such experiments have observed coincident Auger [5,6], threshold photoelectrons [7], and photoelectrons with larger energies [8]. In this work, we present the measurements of Kr^{q+} yields coincident with *K*-shell fluorescence as incident x-ray energy is varied across the *K*-shell threshold.

A major complication to a straightforward interpretation of coincident charge-state spectra is that the threshold vacancy states, one wishes to study, are usually unstable. Hence, the charge states measured reflect a statistical result of subsequent cascade decay to many different charge states from each initial state created. The effects of the cascade can be important [7], and usually cloud direct interpretation of the threshold process. In particular, spectator states that start the cascade with an excited Rydberg electron may either retain or lose the electron. For example, in the measurement of Ar^{q+}, in coincidence with *K-LL* electrons [9], it was found that the yield of Ar^{3+} (which can occur only as a decay product of $[2p^2]np$ spectator states [10]) was less than expected from the calculations of excitation cross sections, since the np spectator electron can be lost in the cascade process. In turn, this loss enhanced the observed Ar^{4+} yields which also arise directly from the decay of the $[2p^2]$ diagram states. To extract the production probabilities for comparison with the theory, it was thus critical to account for cascade spectator loss.

In the present case of Kr *K*-shell fluorescence, the number of charge states is much larger and the problem becomes very complex. However, we distinguish certain regularities in the behavior of the yields as threshold is traversed, and in this work we explore these regularities and seek a general understanding of what lies behind them. Central to this understanding is the question of how normal cascade decay is affected by the presence of a Rydberg electron. In our earlier work [9], it proved tractable (for Ar^{3+}) to account for spectator-electron loss using a simple model of the cascade. Basically, in this model, the spectator electron is assumed to do very little until the end of the cascade, whereupon it may undergo a final participator-Auger step—ejecting an electron with very low kinetic energy. Here, we expand and formulize this model and apply it to the present case.

While the dynamics of threshold excitation is certainly important to the present problem, we find the question of cascade decay involving spectator electrons to be a more vital aspect of the work; an understanding of this behavior goes far beyond the application to the present situation. Photoexcitation near threshold is an important subject, applicable to many branches of physics, and is studied by a wide range of methods. Because the cascade process provides an opportunity for spectator-electron loss, and thus an increase in charge, any study relying on an interpretation of ionic charge states is affected, as in the Ar^{3+}-Ar^{4+} example discussed above. Furthermore, the spectator-loss mechanism provides a source of low-energy electrons, and any study relying on the interpretation of threshold electrons must take

cascade processes into account. An example of such a case is the interpretation of double $3p$ ionization in Ar, where the cascade (indirect) contribution obscures the direct process [11]. There is thus a real need to understand the role of spectator electrons in the cascade processes.

In Sec. II, we outline the experimental details. In Sec. III, we present some general remarks, the results for the coincident ion branching ratios above threshold, and then how these relate to ratios for noncoincident decay of Kr $2p$ vacancies. Next we examine the yields across the threshold where we find that low-q states exhibit noticeable resonance effects. To explain the shape of the partial yields as a function of energy, we develop a model of the cascade process and a method to fit the data with this model. Armed with this framework to describe the observed yields, we discuss why our results seem reasonable and suggest some general trends.

II. EXPERIMENTAL METHODS

The experiment was performed on the BESSRC-CAT bending magnet beam line 12-BM [12] at the Advanced Photon Source, Argonne National Laboratory. Synchrotron radiation was monochromatized using a Si(111) double crystal monochromator, providing a focused x-ray beam with a delivered bandpass of approximately 5 eV at $h\nu \approx 14.3$ keV, comparable to the natural K-shell width of the Kr target atom (≈ 2.7 eV).

The incident x rays were focused onto a Kr gas jet, located at the source region of both an ion time-of-flight (TOF) spectrometer and a x-ray fluorescence detector. The background pressure in the chamber was maintained at 6×10^{-5} Torr (corrected ion-gauge reading) by applying a 5 Torr backing pressure to the gas needle with a Baratron metering system. This arrangement was found optimal in maximizing count rates, while showing no pressure-dependent effects in the ion spectra; at higher pressures charge-exchange effects were observed in the ion spectra. The flux of the incident x-ray beam was measured with an ionization chamber.

The ions created in the source region were accelerated electrostatically in a TOF spectrometer to energies of 5 keV/q, and detected by a microsphere plate (MSP) biased at 3.2 kV. The x rays emitted in the source region were detected with an avalanche photodiode (APD). The APD was mounted outside the vacuum chamber at right angles to the plane of polarization, located approximately 2 cm from the source region and had an active area of 1 cm^2 providing a solid angle $\sim 2\%$ of the total sphere. The x rays reaching the APD traversed a Kapton window, air gap, and Be window—effectively filtering out lower-energy fluorescence from the outer Kr shells. While the fast APD pulse (rise time $\leqslant 1$ ns) gives excellent timing results, its low-energy resolution precludes any means of distinguishing between K_α and K_β fluorescence. While this fact must be kept in mind for any detailed analysis, the K_α decay channel is quite dominant ($\approx 87\%$) and for most descriptive purposes the K_β decay channel can be ignored.

The ion TOF charge-state spectra, coincident with a K-shell fluorescence photon, were measured by using the fast APD photon signal as a start pulse for timing electronics (both time-to-digital and time-to-amplitude converters) and the ion TOF signal as a stop. Figure 1(a) displays an example of a coincident TOF ion spectrum, recorded with the incident-photon energy set slightly below (-1.9 eV) the Kr K-ionization threshold. (In this work, we report all incident-photon energies relative to the Kr K-ionization threshold I_K, nominally 14 327.2 eV [13]. Our determination of this threshold location in terms of our experimental, relative photon energy scale is discussed in a later section.) Charge states from Kr^{1+} up to Kr^{8+} are easily resolved, and for the lower charge-states peak structures due to the various Kr isotopes are also apparent.

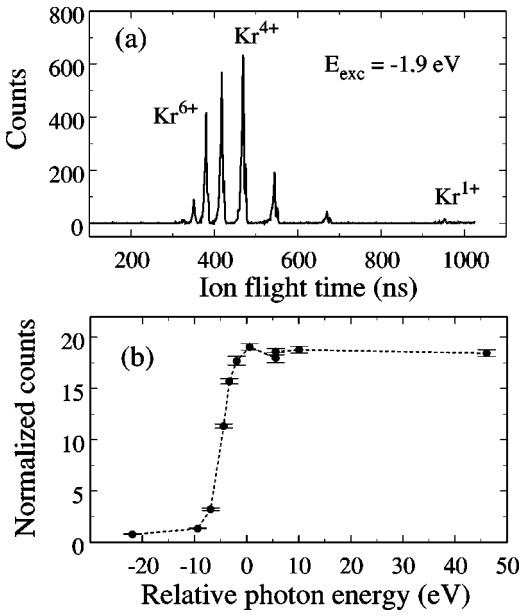

FIG. 1. (a) Typical ion time-of-flight spectrum, coincident with $K_{\alpha,\beta}$ fluorescence. Here, the incident-photon energy was tuned 1.9 eV below the K-shell ionization threshold. (b) Total coincident ion counts normalized by the incident flux as a function of photon energy relative to the K-shell threshold.

From Fig. 1(a), it is seen that the flight time of a typical ion is of the order of 300–700 ns, long in comparison with the bunch spacing of the APS storage ring (153-ns spacing between individual bunches). However, random events produced only a minimal background due to the low cross section. Typical coincident count rates were of the order of 2–35 Hz, in comparison to noncoincident count rates of 10–170 Hz for fluorescence (APD) and 1–10 kHz for ions (MSP).

Figure 1(b) displays the total number of coincidence counts normalized by incident flux as a function of incident-photon energy. The total yield in Fig. 1(b) is proportional to the cross section for $K_{\alpha,\beta}$ emission.

III. RESULTS AND DISCUSSION

A. General remarks and features

The states of interest in this work are photoexcited states that include a fluorescence photon whose energy meets the coincidence requirement. The theory of resonant-Raman and

resonant-fluorescence scattering describes the excitation of such states [1,3]. Their creation (e.g., $[2p]+K_\alpha$) is seen as arising from coupling with virtual, intermediate resonance states—in this case the $[1s]xp$ ($x=n$ or ε) states. Hence the process is described as an inelastic photon scattering event: diagram or resonant-fluorescent scattering $\mathrm{Kr}+h\nu_{in} \rightarrow \mathrm{Kr}^{+}[2p]+h\nu_{out}+e^{-}$, or resonant-Raman scattering $\mathrm{Kr}+h\nu_{in} \rightarrow \mathrm{Kr}^{*}[2p]np+h\nu'_{out}$. However, in this work the low APD resolution precludes any possibility of observing line-shape effects, distinguishing between the diagram (resonant fluorescent) K_α and the Raman satellites, or even between K_α and K_β channels.

Because of this averaging, we are only concerned with the relative cross sections for production of states that will begin the ensuing cascade. Because relaxation effects between the resonant (intermediate state) xp and the excited np or εp orbitals are very small, to a good approximation these cross sections factorize into products of excitation and decay terms and the process can be pictured as a ''two-step'' process:

$$\mathrm{Kr}+h\nu_{in} \rightarrow \begin{cases} \mathrm{Kr}^{+}[1s]+e^{-} \rightarrow \mathrm{Kr}^{+}[2p]+h\nu_{out}+e^{-} \\ \mathrm{Kr}^{*}[1s]np \rightarrow \mathrm{Kr}^{*}[2p]np+h\nu'_{out}. \end{cases} \quad (1)$$

Hence, although the process is really a one-step resonant scattering event, for the purposes of this work, we can safely regard it in the old light as two step—with our coincidence condition picking out only events that proceed along the pathways of Eq. (1).

From either viewpoint (one step or two step), the charge states we measure in coincidence with x-ray emission result from the cascade decay of excited $[2p]np$ or ionized $[2p]$ states (and to a lesser extent, the corresponding $[3p]$ states from the $K_{\beta_{1,3}}$ coincidences). The point of the above discussion is that, since the two-step approximation is accurate within the present context, we can regard the cross sections for producing $[2p]$ and $[2p]np$ states as simply proportional to σ^{+} and σ^{*}_{np}, the cross sections of the $[1s]$ and $[1s]np$ states, respectively. Note that this simple picture does not hold in the radiationless decay channels where the relaxation effects are strong [9].

At a given incident-photon energy, the coincident yield of Kr^{q+} ions depends on the cross section for producing $[2p]$ and $[2p]np$ states and their respective probabilities [P^q and $P^q(np)$] of subsequent cascade decay to a stable Kr^{q+} ionic ground state:

$$\mathrm{Kr}+h\nu_{in} \rightarrow \left\{ \begin{array}{l} \sigma^{+} \quad P^q \\ \rightarrow [2p] \rightarrow \mathrm{Kr}^{q+} \\ \sigma^{*}_{np} \quad P^{q(np)} \\ \rightarrow [2p]np \rightarrow \mathrm{Kr}^{q+} \end{array} \right\} + \text{coincident photon}. \quad (2)$$

Typically, a coincidence condition imposed on an experiment aids in simplifying the spectra under consideration [5]. The present case is another such example and, by selecting only the decay channels outlined in Eq. (2), the number of charge states observed is much reduced from noncoincident spectra excited above the *K* edge [14], where charge states as high as $10+$ have been observed.

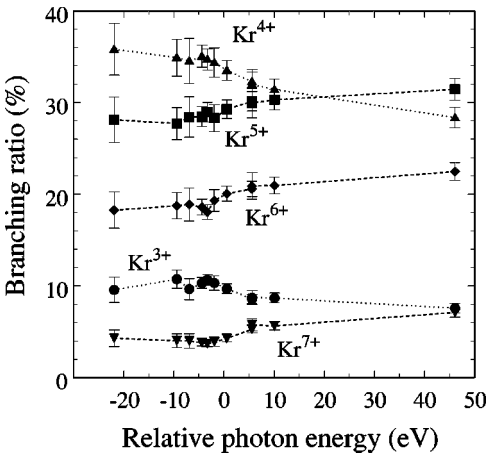

FIG. 2. Branching ratios for the dominant coincident Kr^{q+} charge states as a function of incident-photon energy relative to the threshold. Lines connect the measured points to better indicate the variation with energy.

The ion TOF spectra, recorded at various energies across threshold, were analyzed by comparing the different peak areas to the total area. If the MSP detection efficiency is not dependent on the ionic charge, this procedure gives a direct measure of the branching ratios of the various ionic states in coincidence with $K_{\alpha,\beta}$ emission. The measurements of test spectra using a lower TOF acceleration voltage (3.3 kV) resulted in statistically the same branching ratios, implying that the MSP was being operated in the saturated range.

The Kr^{q+} branching ratios as a function of incident-photon energy are displayed in Fig. 2. The general results of the experiment are clear from the figure, i.e., a gradual tendency for the higher-charge states to be enhanced as the threshold is traversed, with a corresponding suppression of the low-charge states.

There are several regimes of relative (or excess) photon energy ($E_{exc}=h\nu_{in}-I_K$) of interest, distinguished by the kinds of resonance states excited. These energy regions can be quantified from the analysis of the Kr *K*-absorption edge by Breinig *et al.* [13], where the edge is partitioned into excitation to discrete $[1s]np$ states below threshold ($E_{exc}<0$) and a smooth edge with inflection point at threshold ($E_{exc}=0$), which describes the onset of $[1s]$ ionization. The $[1s]np$ excitation cross sections σ^{*}_{np} can be modeled as Lorentzian functions of natural width Γ_K (dictated by the $[1s]$ hole lifetime). The ionization continuum σ^{+} can be modeled by an arctangent function with inflection point at threshold, and its spread about the threshold is also dictated by Γ_K. The arctangent function arises from assuming a flat $1s$-ionization continuum. This partition of the edge—in terms of virtual-state creation—is quite justifiable within the one-step scattering theory, however, some care must be taken in interpreting experimental results with regard to the *individual* terms of the partition—since they do not (in general) reflect cross sections for individual physical states [9]. With our assumption of the two-step model [Eq. (1)], we proceed by interpreting each partition term as physical.

For energies slightly below the $[1s]$ threshold the neutral $[1s]np$ and singly ionized $[1s]\varepsilon p$ states are both of primary

TABLE I. Experimental $K_{\alpha,\beta}$-coincident branching ratios (in percent) of Kr^{q+} ions following *K*-shell ionization at three energies above threshold. Also included are the measured ratios of Carlson *et al.* [18] following $L_{2,3}$ ionization. The theoretical predictions of (a) Kochur *et al.* [19] and (b) El-Shemi *et al.* [20] are included for both the case of $L_{2,3}$ ionization and when adjusted to reflect the present experimental situation.

	Experiment				Theory			
q	$[K]\rightarrow K_{\alpha,\beta}$ (Present)			$[L_{2,3}]$	$[L_{2,3}]$		Corrected	
	+5.6 eV	+10.1 eV	+46.1 eV	Ref. [18]	*a*	*b*	*a*	*b*
9					0	0.1	0	0.1
8	0.8 (0.3)	0.8 (0.2)	0.9 (0.2)	1.0	1.0	1.0	0.9	0.9
7	5.4 (0.3)	5.6 (0.4)	7.1 (0.5)	8.0	6.8	9.9	5.9	8.6
6	20.7 (0.7)	21.0 (0.9)	22.5 (1.0)	21.0	18.6	18.0	16.1	15.8
5	30.1 (0.9)	30.3 (1.1)	31.4 (1.2)	37.0	29.0	33.6	25.1	31.0
4	32.2 (0.9)	31.4 (1.2)	28.4 (1.1)	29.0	40.7	33.7	35.7	34.6
3	8.6 (0.4)	8.7 (0.5)	7.6 (0.5)	3.0	2.2	2.3	13.4	6.6
2	1.5 (0.2)	1.4 (0.2)	1.3 (0.2)	1.0	1.8	1.4	2.0	1.4
1	0.9 (0.1)	0.8 (0.2)	1.2 (0.5)	<0.5	0	0	1.1	1.1

importance. According to the scheme of Eq. (2), the ionic states that begin the coincident cascade process are $[2p]np$ and $[2p]$. Farther below the $[1s]$ threshold, the singly ionized $[2p]$ states become dominant, although the total cross section is very weak. As threshold is approached from below the cross section increases and, at energies $E_{exc}\approx -3$ eV, the $[2p]np$ states dominate. Below threshold we therefore see a slow change from the yields at low energy up to the excitation region just below threshold. At these energies the data show a hint of structure in the branching ratios.

For photon energies just above threshold (by perhaps $E_{exc}\approx\Gamma_K$), the ionized resonant $[1s]\varepsilon p$ states again become dominant and we expect to observe cascades from the $[2p]$ state only. In this energy regime, we would expect the ion branching ratios to become constant. Furthermore, the yields should closely resemble the distributions expected for noncoincident $L_{2,3}$ ionization. In the following section, we investigate this link more closely.

Finally, for energies $E_{exc}\geqslant 12$ eV more complicated states such as doubly excited $[1s,4p]np\,n'p$, $[1s,4p]np$ and ionized $[1s,4p]$ states are created [15]. As these states become populated, we expect more complicated and highly ionized states beginning the cascade. We might therefore expect that the branching ratios of the higher-charge states will increase again as these new thresholds are exceeded. Although our data include only a single energy ($E_{exc}=+46.1$ eV) in this regime, the expected trend is observed.

B. Above-threshold results

Before investigating the threshold behavior of the ion yields, it is of some interest to examine our observed branching ratios just above threshold. As mentioned in the preceding section, these ratios should be comparable to those occurring as a result of pure $L_{2,3}$ ionization.

The natural width Γ_K of the Kr *K* shell is estimated as 2.75 eV [16], and calculated as 2.71 eV [17]. In considering above-threshold behavior, we thus exclude our data at $E_{exc}=+0.6$ eV, since the $[2p]$ population has not risen to its full value and the $[2p]np$ states still have appreciable intensity. Table I displays our results for incident energies at $E_{exc}=+5.6$ and $+10.1$ eV. Within statistical uncertainty the branching ratios are constant at these higher energies. Also, included for comparison are our results for $E_{exc}=+46.1$ eV. As previously noted, once above the multiple-excitation edges, the higher-charge states ($q\geqslant +5$) have increased in relative yield at the expense of the lower-charge states ($q<+5$).

The experimental results of Carlson *et al.* [18] for $L_{2,3}$ ionization are included in column 5 of Table I. Overall, their results are in reasonable agreement with ours; some differences are apparent but they may be largely related to their method: measurements at several energies using resonance lines, coupled with estimated cross sections to unravel subshell yields (see Ref. [18] and references therein). One notable feature of our above-threshold data is that the coincidence requirement, coupled with a tunable x-ray source, produces a fairly pure $[2p]$ state with only small contamination from $[3p]$ vacancies.

While not listed in the table, we are also in reasonable agreement with the recent threshold Kr L_3 data of Hayaishi *et al.* [7], who have measured ion yields in coincidence with zero-kinetic-energy electrons. While no branching ratios are listed, estimates from their Fig. 1 give rough values of 29%, 33%, and 29% for the yields of Kr^{4+}, Kr^{5+}, and Kr^{6+}, respectively. Comparison with their data cannot be pushed too far, since their electron yields peak at different excess energies for different charge states. These shifts are due to post-collision interaction of the initially ejected $1s$ photoelectron and other electrons ejected during the cascade decay.

The theoretical predictions of Kochur *et al.* [19] and El-Shemi *et al.* [20] are also included in Table I, assuming the cascade begins from an $[L_{2,3}]$ hole state (columns 6 and 7, respectively). Here we have statistically averaged their results over the *j* sublevels. To compare more closely with our data, these values should be adjusted to include decay from $[M_{2,3}]$ and $[N_{2,3}]$ states, corresponding to coincidence with K_{β_1} and K_{β_2} x rays. To do so we use radiative branching

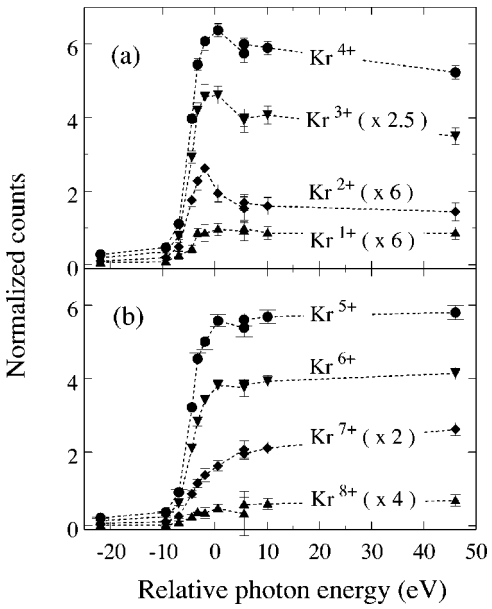

FIG. 3. Flux normalized yields Y^{q+} as a function of incident-photon energy relative to the threshold. Some of the weaker yields have been enhanced by the factor indicated. Note that the units are the same as in Fig. 1(b), and the sum of these yields reproduces the total normalized yield. The lower-charge states ($q=1-4$) are plotted in panel (a), while the higher-charge states ($q=5-8$) are plotted in panel (b).

ratios [from Table II of Ref. [19]: $K_{\alpha_{1,2}}$ (86.7%), K_{β_1} (12.2%), and K_{β_2} (1.1%)] to weight the corresponding charge-state distributions ($L_{2,3}$, $M_{2,3}$, and $N_{2,3}$, respectively) of the two groups. These corrected, theoretical distributions are included in columns 8 and 9. These values do not include any experimental adjustments, e.g., variation of APD efficiency with energy. Note that the major consequence of this correction is the enhancement of the Kr^{3+} abundance due to the highly probable $M_{2,3}-M_{4,5}N$ Coster-Kronig transition followed by $M_{4,5}$-NN (see Ref. [19], Tables II and VI).

C. Threshold behavior

1. Spectator cascade model

Much more insight into the near-threshold behavior can be gained by normalizing the coincident Kr^{q+} yields by the integrated incident flux, as was the total yield of Fig. 1(b). These normalized yields are then proportional to the partial cross sections for observing the various charge states, and their sum results in the total yield of Fig. 1(b). Figure 3 shows the partial yields for states Kr^{1+} up to Kr^{8+}. In the figure, lines between data are included to better indicate the trends, and some of the less intense yields are magnified for better viewing by the factors indicated.

Figure 3 demonstrates that the behavior of the partial yields is different for low- and high-charge states. Figure 3(a) displays the low-charge yields ($q=1-4$); a peak at or just below threshold in the range where the spectator states $[2p]np$ are being created, followed by a slight decrease above threshold. The higher-charge-state yields ($q=5-8$) in Fig. 3(b) show no such feature (discernible within statistics), the yields rise rapidly at threshold and increase gradually thereafter.

It appears then that the role played by the spectator electrons in the presence of a decaying core is of central importance for interpreting the present experiment, at least for the lower-q states. How is it that the decay of initial states such as $[2p]$ differs from that of the $[2p]np$? Why does this vary with charge? To explore these questions in light of our present data, we extend a model previously used to successfully modify *radiationless* resonant-Raman cross sections for cascade effects [9]. In the following, we ignore any effects due to K_β coincidences, and hence the $[3p]$ states.

We consider first all states of an ion Kr^{q+} that are stable against Auger decay, labeled by $\{q,\mu\}$ where $\mu=1,\ldots,N(q)$. (An example for $q=1$ might be the two states $[4p]$ and $[4s]$, with $\mu=1$ and 2, respectively.) Since the decay of these states does not involve electron ejection, they all decay eventually to the ground state $\{q,\mu=1\}$ maintaining the ionic charge q. If the atom is initially prepared in the vacancy state $[2p]$, there is a probability P_μ^q that it will cascade decay to each of the above states. Figure 4(a) represents this process in terms of an energy-level diagram. There is therefore a probability $P^q=\Sigma_\mu P_\mu^q$ that the $[2p]$ hole state will result in a stable ion of charge q. Experimentally, these P^q are the branching ratios measured in the region just above threshold, where the $[2p]$ state is predominantly created.

Next, what happens if the vacancy includes an extra electron, bound in a Rydberg orbital $[2p]np$, as is the case in the threshold region? The excited electron can either be involved or passive in the following decay steps (participator or spectator decay). For deep inner-shell holes, the spectator channels are usually considered very much more likely than the participator channels. For example, the branching ratios for the participator transitions $[2p]np\rightarrow[3l]+e^-$ or $[4l]+e^-$ would be expected to be negligible in comparison to the various spectator Auger transitions. We estimate that $[2p]5p\rightarrow[3d^2]5p+e^-$ spectator decay is roughly 2000 times more likely than the decay by the $[3d]$ participator channel (the strongest participator), and up to 106 000 times more likely than the $[4s]$ route (the weakest). Here we have estimated the relative probabilities by taking a squared ratio of the largest relevant Slater R^k integrals, using configuration-average Hartree-Fock (HF) wave functions. On the other hand, in situations in which there are no possible spectator Auger channels, participator Auger decay can become very intense, completely dominating any radiative spectator-decay channels [21]. Exploiting these two ideas, we proceed with our model by assuming that the excited Rydberg electron remains as a spectator during the cascade decay of the core ion, until finally there are no remaining core-Auger transitions possible.

Clearly this assumption is an overstatement of the actual behavior. For cases in which the inner-shell hole is closer to the valence level, one might expect participator decay to become important. For example, strong participator peaks can be identified in the resonant Ar $[2p]$ spectra [22,23] and in the resonant Kr $[3d]$ spectra [24]. How much of this partici-

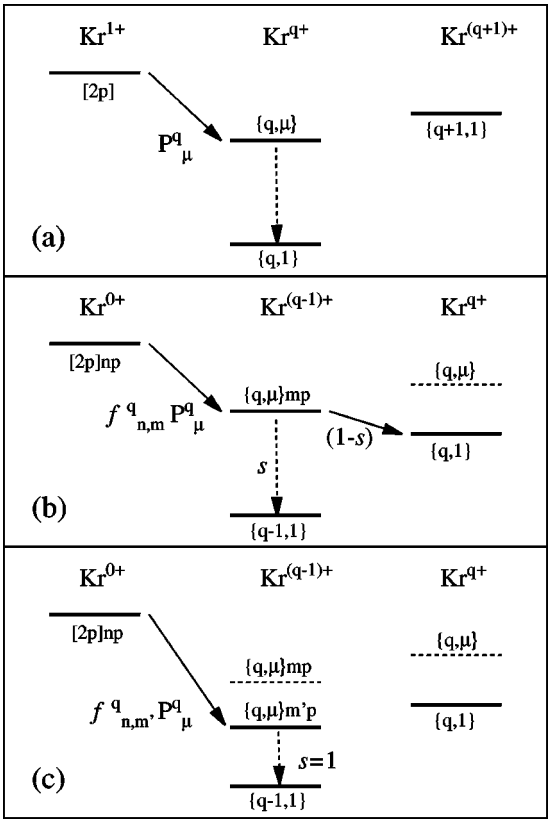

FIG. 4. Schematic outline of the cascade model discussed in the text. (a) Starting from the ionized $[2p]$ hole state, the atom undergoes cascade decay to state $\{q,\mu\}$ (the μth lowest energy eigenstate of the ion Kr^{q+}) with probability P^q_μ. Since this state is lower in energy than $\{q+1,1\}$, the ground state of $Kr^{(q+1)+}$, the cascade leads to a stable ion of charge q. Panels (b) and (c) illustrate decay beginning from the excited state $[2p]np$. By assumption, the np electron plays no active role in the core cascade, hence the probability of reaching the final state $\{q,\mu\}mp$ is the product of P^q_μ and the probability of the np electron "shaking" to the level mp during the core cascade ($f^q_{n,m}$). Adding an additional Rydberg electron to $\{q,\mu\}$ lowers the energy. In panel (b), the state $\{q,\mu\}mp$ is above $\{q,1\}$ so that an additional ionizing step is possible with probability $1-s$. Hence, there is a probability s that the mp electron "sticks," forming a stable ion $Kr^{(q-1)+}$. Panel (c) illustrates the case $\{q,\mu\}m'p$ (with $m'<m$) in which the $m'p$ electron is bound so tightly that it lies below $\{q,1\}$; further ionization is not possible and the sticking probability s becomes unity.

pator intensity can be ascribed (in the two-step approximation) to the direct ionization is not clear. In fact, Lu *et al.* [25] have observed intense $[3p^2]n'd\rightarrow[3p^2]+e^-$ transitions following Ar $[2p]nd$ excitation, indicating that the spectator step $[2p]nd\rightarrow[3p^2]n'd+e^-$ is intense. It has been shown that participator decay is the major decay mechanism in some cases: the $[2p]3d\rightarrow[3s]+e^-$ transition in Mg [26] and the analogous $[3p]3d\rightarrow[4s]+e^-$ transition in Ca [27]. At any rate, it is certain that as vacancies bubble up from the tightly bound shells, and the number of open shells increases, participator channels will increase in importance and finally dominate. So far as we know, there has as yet been no investigation into the systematics of this difficult question. Hence, our assumption is a simplified approximation to the more general behavior we expect. We expect it to be valid for the beginning stages of the cascade, and that these steps largely determine the resulting value of q.

In the ensuing cascade decay we therefore *assume* that the np electron plays no active role; the core decays with the same probabilities as if the Rydberg electron were missing. The probability of the state $[2p]np$ decaying to a state $\{q,\mu\}mp$ (an ion of overall charge $q-1$) is thus $f^q_{n,m}P^q_\mu$. The factor f accounts for the probability that the excited electron, while remaining a spectator to the core decay, can relax to some different level mp in the $(q-1)$ *ionization* steps [Figs. 4(b) and 4(c)]. We make a further approximation that f only depends on the number of such steps, rather than on the particular decay routes taken and the specific final core state μ. While this is not necessary for what follows (a μ dependant f could be included in the averaging carried out below), the approximation allows us an intuitive picture of an isolated spectator electron experiencing a simple shake transition each time the core ionizes.

Finally, we consider the states $\{q,\mu\}mp$ involving an mp Rydberg electron bound to the charged core $\{q,\mu\}$. Depending on the particular core state, there may be a chance for *participator* Auger emission. An example of such a transition is the valence-multiplet transition $[4p^2(^1D)]mp \rightarrow[4p^2(^3P)]+e^-$ or an inner-valence transition $[4s,4p]mp\rightarrow[4p^2]+e^-$ (see Ref. [21]). When such transitions are energetically possible, their decay rates are much larger than those of the radiative channels and thus occur almost exclusively [21]. If such transitions are allowed, then there is thus an additional ionizing cascade step $\{q,\mu\}mp \rightarrow\{q,\mu'\}+e^-$ possible. This situation is illustrated in Fig. 4(b). If no participator Auger channels are possible then the ion decays, but maintains the total charge $(q-1)$ [Fig. 4(c)]. For each state $\{q,\mu\}mp$, we can assign a microscopic sticking probability $s(q,\mu;mp)$ that the mp electron stays with the core in the final decay step. The microscopic sticking probability is analogous to the fluorescence yield of the state $\{q,\mu\}mp$, but expanded to include the probability of all nonionizing decay possibilities to the stable final state (e.g., the final decay step may really be a series of radiative cascades such as $mp\rightarrow m's+h\nu\rightarrow$etc.).

With these assumptions, the probability that the atom initially prepared in the state $[2p]np$ will decay to an ion of charge q is

$$P^q(np)=P^q\{1-\overline{S}_q(np)\}+P^{q+1}\overline{S}_{q+1}(np). \qquad (3)$$

Here, $\overline{S}_q(np)$ is the average sticking probability of the np electron to the ionic core of charge q. Equation (3) states the obvious results of the model; Ions of charge q can occur in two ways (a) by decay to a *core* state q with a loss of the spectator electron (probability $1-\overline{S}_q$), or (b) by decay to a $q+1$ core with the spectator electron sticking (probability $\overline{S}_{q+1}$).

The average sticking probability is

$$\overline{S}_q(np)=\frac{1}{P^q}\sum_{\mu=1}^{N(q)}P^q_\mu\sum_m f^q_{n,m}s(q,\mu;mp). \tag{4}$$

While the microscopic sticking probabilities $s(q,\mu;mp)$ depend only on the properties of the final state, the average $\overline{S}_q(np)$ additionally depends on the details of the cascade decay. In particular the shake probability $f^q_{n,m}$ depends on the number of ionizing steps $(q-1)$. Because shake up and shake down is so likely during ionization, $f^q_{n,m}$ becomes a fairly broad function of m about n—even for only a few steps. Due to this averaging, we expect $\overline{S}_q(np)$ to vary slowly with n.

We have employed a fairly idealized physical model to arrive at Eq. (3) which relates the probabilities $P^q(np)$ (that the excited state $[2p]np$ decays to a stable ion of charge q) to the probabilities P^q pertaining to the decay of the ionized state $[2p]$. What is perhaps not obvious at this point is that almost any new probability distribution Q^q can be derived from the distribution P^q by the formal relation $Q^q=P^q(1-\rho_q)+P^{q+1}\rho_{q+1}$. This transformation of $P^q\rightarrow Q^q$ preserves the normalization $\Sigma_q Q^q=\Sigma_q P^q=1$ for any choice of the parameters ρ_q, and the requirement that Q^q should represent probabilities $(Q^q\geqslant 0)$ puts only a modest restriction on them. From our physical definition of P^q we must have $P^0\equiv 0$ and $P^q=0$ when $q>q_{\max}$, so the only restriction on Q^q is that $Q^q=0$ for $q>q_{\max}$. Hence, Eq. (3) can be used to define the parameters $\overline{S}_q(np)$ (for $q=1,\ldots,q_{\max}$) in a broader sense, though there is little motivation to do so without the ideas outlined above.

In what follows, therefore, $\overline{S}_q(np)$ can be regarded as describing the dynamic relation between the above-threshold charge distribution and that originating from the excited state $[2p]np$. They form a set of parameters with which we hope to systematize any generalities lurking in the physics, which might not be apparent from a comparison of specific experimental charge distributions. Our model outlined above, based on the idea of microscopic sticking probabilities, provides a reference point to examine the true nature of $\overline{S}_q(np)$ in terms of our intuitive ideas [and Eq. (4) provides a model-based method for calculating them]. In what follows, we therefore continue to lean heavily on our model, but the more general nature of $\overline{S}_q(np)$ should be borne in mind—particularly for future work.

Before proceeding with our development, a few remarks concerning the generalized nature of the sticking probabilities are worth noting. First, for an arbitrary probability distribution Q^q the transformation parameters are $\rho_{k+1}=\Sigma_{q=0}^k(Q^q-P^q)/P^{k+1}$. Hence, the parameters ρ_q can generally be positive or negative and quite large in magnitude, i.e., they need not look like probabilities. If it is physically the case that $0\leqslant\overline{S}_q(np)\leqslant 1$ for all q, then the interpretation of $\overline{S}_q(np)$ as probabilities of the spectator-electron ''sticking'' is legitimate for intuitive purposes, and our model's validity is strengthened. From Eq. (3) alone, we expect that $\overline{S}_q(np)\rightarrow 0$ as $n\rightarrow\infty$, so that $P^q(np)\rightarrow P^q$ in the same limit. We might also expect that $\overline{S}_q(np)$ deviate from zero to the largest degree for the lowest possible values of n, where the spectator electron is most strongly coupled to the ionic core. Finally, we note from the general transform that $\langle q\rangle_Q=\langle q-\rho_q\rangle_P$. Hence $\overline{S}_q(np)$ are connected with the difference in average charge resulting from spectator and parent-ion decay:

$$\langle q\rangle_{[2p]np}=\langle q\rangle_{[2p]}-\sum_q\overline{S}_q(np)P^q. \tag{5}$$

To predict the flux-normalized partial yields of Fig. 3, the probabilities for the population of each initial state must be included: (a) σ^+, the probability for population of the state $[2p]$; as a function of incident-photon energy near threshold, it is usually approximated by an arctangent function (see Ref. [13]); (b) σ^*_{np}. The probabilities for creation of the spectator states $[2p]np$, considered in this work as Lorentzian functions centered at their respective resonance energies just below threshold. The total cross section $\sigma_T=\sigma^+ +\Sigma\sigma^*_{np}$ describes the total yield of Fig. 1(b). The partial yields are a sum of products of excitation and decay probabilities for each state created near threshold: $Y^q=P^q\sigma^+ +\Sigma_n P^q(np)\sigma^*_{np}$. These can be rewritten as

$$Y^q=P^q\sigma_T+\sum_n\sigma^*_{np}\{P^{q+1}\overline{S}_{q+1}(np)-P^q\overline{S}_q(np)\}. \tag{6}$$

The widths of the above resonant-cross-sections are dictated by the natural width of the state from which the $2p$ hole is derived. In the present case of Kr $[2p]$ states, originating from the decay of the Kr $[1s]$ hole states by K_α emission, the width is $\Gamma_{[1s]}\approx 2.7$ eV. Furthermore, the energy dependence of all cross sections must be convoluted with the beam line bandpass, here ~ 5 eV. Because this width is large compared to the distribution of resonance energies, each σ^*_{np} overlaps in energy and only the first few contribute substantially to the total excitation cross section $\sigma^*\equiv\Sigma\sigma^*_{np}$. For Kr, the σ^*_{5p} is dominant [13]. Because of this, and the fact that $\overline{S}_q(np)$ are expected to be weak functions of n, we can make the final approximation:

$$Y^q\approx P^q\sigma_T+\{P^{q+1}\overline{S}_{q+1}-P^q\overline{S}_q\}\sigma^*, \tag{7}$$

where $\overline{S}_q$ now reflects a cross-section weighted average of $\overline{S}_q(np)$ over the lower-n states.

Within this last approximation, the energy dependence of each of the yields (Fig. 3) is a composite of two terms: first, the total cross section σ_T [Fig. 1(b)] weighted by the above-threshold branching ratio P^q, and second a term proportional to the total excitation cross section σ^* which peaks just below threshold. It is the magnitude of this second term which causes the differences in yield profiles; a positive contribution superimposes a resonance peak to the smooth edge shape, while a negative contribution subtracts from the edge and produces no noticeable structure.

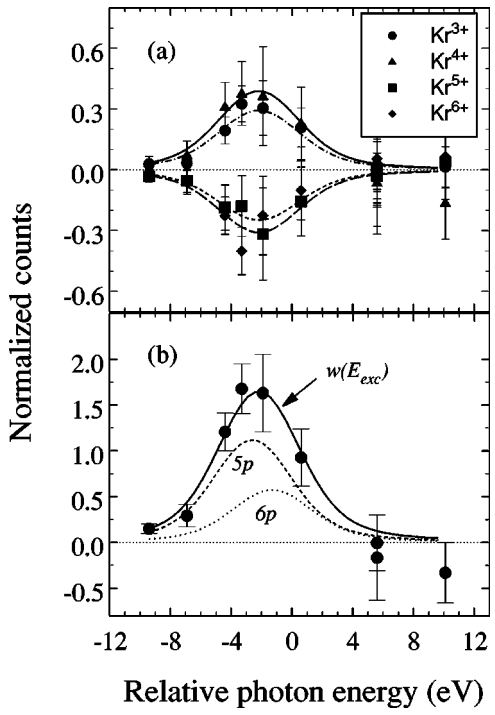

FIG. 5. (a) Examples of the residual yields R^{q+}, each formed by subtracting a scaled total yield (Fig. 1) from the partial yields Y^{q+} of Fig. 2. For clarity, we include only a few of the charge states. The curves are fits to the data as discussed in the text. (b) The sum of $|R^{q+}|$ over q. To this data is fit a model of the total photoexcitation cross section $w(E_{exc})$. The contributions to this total from the $5p$ and $6p$ resonances are also displayed.

2. Threshold analysis

The results of the preceding section provide an explanation for the various energy dependences of the yields in Fig. 3. The simple form of Eq. (7) also suggests hope for extracting some rough information about the average sticking probabilities from the data. To do so, some model function for the excitation cross section σ^* is needed. One is initially tempted to perform a least-squares edge fit along the lines of Breinig *et al.* [13]; σ^+ is modeled as an arctangent (with inflection point at threshold, $E_{exc}=0$, determined by the fit), and σ^* is modeled as a superposition of Lorentzians (whose relative intensities and energies are determined by the fit). In practice, however, we find the method very unstable. Fits for the relative intensities of the Lorentz functions are extremely sensitive to slight changes in the (fixed) threshold energy used. Additional sensitivities to changes in other parameters (natural width, band pass, and resonance energies) compound the problem. Instead we employ a different method based on the form of Eq. (7), which we find to be stable.

As a starting point, we use the data Y^q (Fig. 3), σ_T [Fig. 1(b)], and the observed values of P^q from the above-threshold region (Table I) to form the residual yields

$$R^q = Y^q - P^q \sigma_T . \tag{8}$$

Figure 5(a) displays the residuals as a function of incident-photon energy for several prominent q. All residual yields show either a positive or negative ''resonance'' peak just below threshold. From the model outlined in the preceding section $R^q = C^q \sigma^*$, where the proportionality constants are $C^q \equiv P^{q+1}\overline{S}_{q+1} - P^q \overline{S}_q$. We use this fact with the data of Fig. 5(a) to extract the constants C^q, and hence the average sticking probabilities.

While $\Sigma_q R^q = 0$ identically, the sum $\Sigma_q |R^q| = C\sigma^*$ provides a useful set of (smoother) data with which we fit a function $w(E_{exc}) = C\sigma^*$, where $C = \Sigma_q |C^q|$. This absolute-value sum of the residual yields is displayed in Fig. 5(b).

The function w was determined from the data of Fig. 5(b) using a simple theoretical model of σ^*, a $5p$, $6p$, ... Rydberg series of Lorentz functions, each of natural width $\Gamma_K = 2.72$ eV and convoluted with a Gaussian bandpass function of full width at half maximum $=5$ eV. The energies of each peak relative to a variable threshold value were fixed, consistent with Hartree-Fock $[1s]np$ binding energies. The relative intensities of the resonances for $n>6$ were fixed by quantum defect (n^{-3}) scaling. The relative intensities between the peaks ($n=5,6$, and $n>6$) and the threshold location ($E_{exc}=0$) were determined from a least-squares fit to the data of Fig. 5(b). The resulting function w is shown by the solid curve in Fig. 5(b). Included in the figure are the fitted contributions to w from the $5p$ and $6p$ resonances. As a side note, our fit gives a ratio of excitation cross sections $\sigma^*_{5p}/\sigma^*_{6p} = 2.0 \pm 0.1$ (peak values). Estimating the same ratio from Fig. 5 of Breinig *et al.* [13] gives a value of ≈ 3.

Once a suitable excitation function was determined, a simple least-squares fit of w to each of the residual yields of Fig. 5(a) determined the relative values C^q/C. From these, the *relative* values of the sticking probabilities were extracted by recursion. The recursion can proceed in either the forward or the backward direction, with errors propagating in the respective directions. There is good reason to expect $\overline{S}_1 = 0$ (following section), whence the forward recursion goes as

$$\frac{\overline{S}_q}{C} = \frac{1}{P^q}\left[\frac{C^{q-1}}{C} + \frac{C^{q-2}}{C} + \cdots + \frac{C^1}{C}\right]. \tag{9}$$

Alternately, a similar backward recursion can be started assuming $P^{(9)} = 0$. This assumption is based on the above-threshold spectra where no $q=9$ charge state was discernible (within statistics), and also on theory [19,20].

Finally, $\overline{S}_q$ were determined from the relative values by estimating the unknown constant C from the data. Since $\sigma^*/\sigma_T \approx 1$ when (or if) the excitation cross section is large compared to the ionization cross section ($\sigma^* \gg \sigma^+$), we have $w/\sigma_T \approx C$ there. This situation is roughly realized just below threshold where σ^* peaks and the corresponding ratios of the data proved constant in that region. This estimate of C provides a lower bound for the derived $\overline{S}_q$. Our results are listed in Table II for $\overline{S}_q$ using both the forward and the backward recursion schemes discussed above, as well as our values of the relative C^q.

From the viewpoint of the general definition of the parameters $\overline{S}_q$ discussed above, it is of some significance that ex-

TABLE II. Fit results for the parameters used in modeling the partial yields of Fig. 3. The values of C^q/C indicate the degree to which resonance cross section is added (or subtracted) to the normalized total. The average sticking probabilities $\overline{S_q}$, derived from the former parameters by either forward or backward recursion, are also displayed. These are interpreted as the average probability that an initially excited Rydberg electron survives $q-1$ cascade decay steps and remains bound to the ionic core

q	C^q/C	$\overline{S_q}$	
		Backward	Forward
8	-0.022 (0.005)	0.28 (0.12)	0.17 (1.25)
7	-0.146 (0.020)	0.33 (0.05)	0.31 (0.19)
6	-0.187 (0.045)	0.18 (0.03)	0.17 (0.04)
5	-0.150 (0.052)	0.17 (0.03)	0.17 (0.02)
4	$+0.236$ (0.055)	0.09 (0.03)	0.08 (0.01)
3	$+0.178$ (0.030)	0.11 (0.11)	0.09 (0.02)
2	$+0.090$ (0.014)	0.01 (0.66)	-0.05 (0.06)
1	-0.007 (0.008)	0.10 (1.11)	

perimentally they all are consistent (within error) with our spectator-model interpretation of them as probabilities. The average charge in the above-threshold region is $\langle q\rangle_{[2p]} = 4.78 \pm 0.02$ and $\langle \overline{S_q}\rangle_{[2p]} = 0.15 \pm 0.02$, which from Eq. (5) we interpret as the decrease in the average charge that would result from the (average) presence of a spectator electron. In the following section, we discuss the observed results for $\overline{S_q}$ within the context of our spectator-decay model of the cascade process.

3. Discussion

The $q=1$ charge state is a special case in the scheme outlined above. In this case, one considers zero ionizing decay steps, and therefore must consider participator decay at each cascade step since its probability may be large in comparison to any of the radiative cascade steps.

Starting from the $[2p]$ initial state, a $q=1$ final state can be reached by direct $[2p] \rightarrow [4s] + h\nu$ fluorescence or by some radiative cascade route, e.g., $[2p] \rightarrow [3d] + L_\alpha \rightarrow [4p] + h\nu + L_\alpha$. The sticking probability $\overline{S_1}$ is the probability that starting from a state such as $[2p]5p$, and *given* $q-1=0$ *ionizing* core decay steps, the $5p$ electron will remain attached to a final single-hole core. Our model examines the probability of the participator Auger decay involving the $5p$ orbital after the main cascade process. However, with no core ionizing steps to consider, the evaluation must include participator decay involving all the likely single-hole cores, including $[2p]5p \rightarrow [3l \text{ or } 4l] + e^-$ as well as transitions such as $[3d]5p \rightarrow [4l] + e^-$. While the Auger rates for these participator transitions are weak in comparison with the core-Auger decay, their probability in comparison with *radiative* routes to a stable $[4l]5p$ state would be expected to be large. On this basis, we expect $\overline{S_1} \approx 0$, and have used this fact for the forward recursion analysis. Backward recursion confirms that $\overline{S_1}$ is small but with very large error.

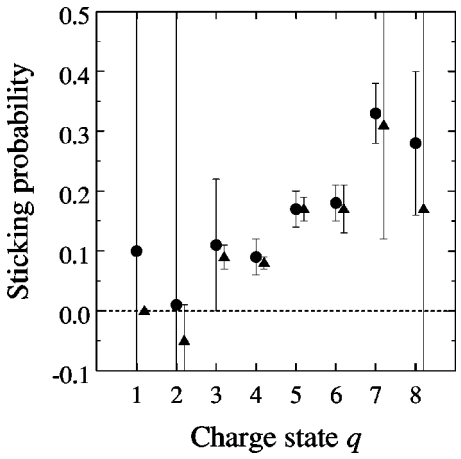

FIG. 6. Average sticking probabilities $\overline{S_q}$, extracted from fits to the residual yields by either forward (triangles) or backward (circles) recursion. These are the average probabilities that a Rydberg electron will survive $q-1$ core ionizing cascade steps and remain attached to the final ion.

Furthermore, some of the limitations of the experiment must also be kept in mind. The theoretical entries of Table I (corrected) suggest that the K_β-coincident events are the dominant contributors to the $q=1$ yield. Hence our model should also include the likelihood of such transitions as $[3p]5p \rightarrow [4l] + e^-$. In this case similar arguments apply as in the $[2p]$ case, again suggesting $\overline{S_1} \approx 0$. The decay model can be easily extended to consider many initial states, but the meaning of $\overline{S_q}$ becomes mostly statistical, losing any intuitive value. In the following, we focus on the results for charge states that are more dominant, where the trends are associated predominantly with K_α coincidences and $[2p]$ initial states.

Figure 6 displays the results of Table II to better indicate the behavior of $\overline{S_q}$ as a function of charge q. The errors for the weaker charge states are large, however, it is still apparent that the probabilities tend to increase with q. At first glance, this trend is reasonable: one might expect a Rydberg electron to be more tightly bound (stuck) to a higher-charge core. However, there are a number of subtleties to consider. First, the sticking probabilities depend, not only on the nature of the final state, but also on the decay routes taken to arrive there. Hence, implicit in our expectations is the major assumption already built into the model; the excited electron remains passive during core decay. Second, since the participator transitions can only occur if there are several final core states, one might expect $\overline{S_q}$ to vary with the number of possible core final states. If one considers only states made from the $4s$ and $4p$ shells, the number of possible states rises from 28 ($q=2$) to 70 ($q=4$), and thereafter decreases. One might therefore expect $\overline{S_q}$ to show a minimum at $q=4$. Finally, it is also commonly known that Rydberg orbitals are not true spectators when the core charge increases, but shake to different levels. In general, it is most likely that an electron in an np orbital will shake up to mp, where $m>n$ (see Refs. [28,29]). This effect tends to negate the idea of increased charge being responsible for increased sticking—the larger q,

TABLE III. Allowed participator Auger transitions for some core configurations of Kr^{q+}. When allowed energetically, the possible np transitions are displayed to the right of the core. For ground configurations, only valence-multiplet (vm) transitions such as $[4p^2]({}^1D)np \rightarrow [4p^2]({}^3P)+e^-$ are possible. For excited configurations, it is sufficient to consider the possibility of inner-valence (iv) transitions, e.g., $[4s4p]np \rightarrow [4p^2]+e^-$. The $5p$ and $6p$ states, which are those primarily excited near threshold, are set in boldface to emphasize their predominance. The fewer the allowed transitions, the greater is the average sticking probability for the charge state q.

q	Ground	vm		iv		iv
Kr^{2+}	$[4p^2]$	**6p**, ...	$[4s4p]$	**5p,6p**, ...	$[4s^2]$	**5p,6p**, ...
Kr^{3+}	$[4p^3]$	$8p$, ...	$[4s4p^2]$	**5p,6p**, ...	$[4s^24p]$	**5p,6p**, ...
Kr^{4+}	$[4p^4]$	$9p$, ...	$[4s4p^3]$	**6p**, ...	$[4s^24p^2]$	**5p,6p**, ...
Kr^{5+}	$[4p^5]$		$[4s4p^4]$	$7p$, ...	$[4s^24p^3]$	**5p,6p**, ...
Kr^{6+}	$[4p^6]$		$[4s4p^5]$	$8p$, ...	$[4s^24p^4]$	**6p**, ...
Kr^{7+}	$[4s4p^6]$		$[4s^24p^5]$	$8p$, ...		
Kr^{8+}	$[4s^24p^6]$					

the less bound we might expect to find the final mp electron since it has been shaken up as many as $q-1$ times.

The behavior of the $\overline{S_q}$ can be explained, within the context of our decay model, as a result of an interplay between all the effects mentioned above. To see how the observed trend can come about, we consider our model's implications using the simplest assumptions possible.

Because all the resonance states are crowded within an energy region comparable to the resonance width, the $5p$ and $6p$ states are the major contributors to $\overline{S_q}$ over all energies. Also, this crowding allows for the approximation leading from Eq. (6) to Eq. (7), where $\overline{S_q}$ becomes the (energy independent) average of $\overline{S_q}(nl)$ weighted by their respective oscillator strengths. Using our fit results of σ^* [Fig. 5(b)], we then have $\overline{S_q} \approx 0.66\overline{S_q}(5p)+0.34\overline{S_q}(6p)$.

Next, we consider how $5p$ or $6p$ electrons, having survived the decay to a core of charge q, can be lost by a participator Auger step. This depends on the particular core state. If the core is in its ground configuration then only the transitions between multiplet states are possible, e.g. ($q=3$) the valence-multiplet [30] transition $[4p^3]({}^2P)np \rightarrow [4p^3]({}^2D)+e^-$. For excited configurations, there is also a possibility of transitions to lower-energy configurations, e.g., the inner-valence [30] transition $[4s4p^2]np \rightarrow [4p^3]+e^-$. These types of transitions are energetically possible if the difference between the initial and the final core-state energies is greater than the binding energy of the np electron. As q is increased, the np binding energy increases, however, the spread of core multiplet energies, as well as the separations between core configurations, remain roughly constant. Hence, as q increases the lower np transitions become cut off. It is in this sense that we can make the above connection between tighter binding and increased stability (sticking).

Table III illustrates the above ideas. For each charge state Kr^{q+}, are listed the core configurations possible by only considering arrangements of $4s$ and $4p$ electrons. Beside each configuration, we list the possible np electrons that can undergo participator Auger decay from that configuration. These values are obtained by comparing single-configuration Hartree-Fock np binding energies with the maximum LS multiplet or inner-valence energy differences. Table III is an oversimplification, yet it demonstrates the general result that as q is increased, much of the low-n participator decay becomes cut off. One can see the general trend in $\overline{S_q}(np)$ from the table; sticking probabilities tend to increase with q.

Finally, we must also consider the effects of shake up on the values of $\overline{S_q}(np)$. For the $5p$ level, the effect is to increase the likelihood of ending in a higher-n level, and hence to decrease the sticking probability. As an example, the probability that the $5p$ electron ends up in the $5p$ level ($f^q_{5p,5p}$) is calculated to be 74% for $q=2$ and decreases to 52% by $q=8$ (estimated from HF shake calculations). The overall effect is to decrease the sticking probabilities, the decrease being larger for the higher q states.

While a calculation of the average sticking probabilities [Eq. (4)] is beyond the scope of the present work, it is worth a brief discussion of what would be involved (and some possible shortcuts) in such an undertaking:

The microscopic sticking probabilities $s(q,\mu;mp)$ must be calculated for each state. Formally this requires calculation of all decay rates for each state. However, this sort of calculation is not necessary. If the mp electron is bound tightly enough, so that any Auger decay is cut off, then $s=1$. For states of m sufficiently large, so that Auger decay is energetically possible, it is a good approximation to assume $s=0$ [21]. The question becomes a matter of comparing relative energies, and the role of $s(q,\mu,mp)$ then reduces to determining a maximum for the summation of $f^q_{n,m}$ over m [9].

The probability of relaxation ($f^q_{n,m}$) of the np to the mp orbital during $q-1$ ionizing steps could be estimated from shake calculations [9]. In this approximation, the f^q can be calculated recursively:

$$f^{q+1}_{n,m}=\sum_{m'} f^q_{n,m'}\langle m'p;q|mp;q+1\rangle^2. \tag{10}$$

We have found that HF calculations become difficult due to

the large values of m required; however, the use of hydrogenic overlaps [29] provides a useful guide to the systematics.

Perhaps the most challenging aspect of the calculation of $\overline{S_q}$ is the determination of the core decay probabilities P_μ^q. For example, given decay to $q=2$, what are the relative probabilities for reaching the various states such as $[4s,4p]({}^{1,3}P)$ and $[4p^2]({}^1S,\ {}^1D,$ or $ {}^3P)$? However, large-scale calculations have been performed for the total P^q [19,20], so calculations for the subprobabilities exist.

Finally, returning to the basic experimental observation: Why is it that the low-q states show a resonance feature in their partial yields Y^q, and how do $\overline{S_q}$ relate to these shapes?

Mathematically, the partial yield Y^q will show a peak when $(P^{q+1}/P^q)>(\overline{S_q}/\overline{S_{q+1}})$. If $\overline{S_q}$ is an increasing function of q, the right side of the inequality will be less than unity. For the low-q charge states, which in this case are weak but grow in strength monotonically with q, the condition is easily met and a resonance peak adds to the scaled total. Once past the strongest charge state the condition is less likely to be fulfilled and the resonance peak subtracts from the total. Since this occurs where the total cross section is rising, the effect is less visible, merely shifting the inflection point of the smooth curve to higher energies.

Less formally, the question simplifies to a matter of ''comes in'' versus ''goes out.'' The charge state Kr^{q+} loses total probability (to $Kr^{(q-1)+}$) when a spectator is excited and sticks, and gains probability from spectators that stick to the $Kr^{(q+1)+}$ core. If the probability (in the absence of spectator excitation) for Kr^{q+} is much smaller than that for $Kr^{(q+1)+}$, then in the energy region where spectators are excited we expect an overall increase in the total yield of Kr^{q+}.

IV. CONCLUSION

In summary, we have measured Kr^{q+} ion charge-state spectra in coincidence with K-shell fluorescence across threshold. Above threshold the branching ratios are found to be in reasonable agreement with the experimental and the theoretical predictions for Kr $L_{2,3}$ ionization. Near threshold we observe variations in the branching ratios as a function of energy. These variations are connected with different functional forms of the normalized partial yields (cross sections) for each q. The lower-q yields show a resonance peak near threshold superimposed on a smoothly rising edge, whereas the large-q yields show only the smooth rise.

To understand the behavior of these threshold effects, we have introduced a simple model of the decay process in which decay of the photoexcited states is correlated with that of the photoionized states. This is allowed for a simple parametrization of the partial yields, and fits to the model yielded the physical quantities of our formalism: the sticking probabilities $\overline{S_q}$. Although they can be defined with a broader meaning [Eq. (3)], in the current work we consider them as an average probability that an excited Rydberg electron stays with its ion as the ion cascades to a final state of (core) charge q, and remains attached thereafter. These probabilities were found to (roughly) increase with q, and we have presented a general discussion as to why this should be the case.

From these arguments and results, we have tentatively concluded that the increase of $\overline{S_q}$ with q should be a general trend for all systems. We also speculate that, in general, if the probability (in the absence of spectator excitation) for charge state q is much smaller than that for $(q+1)$, then near threshold the partial yield for $q+$ will show the resonance enhancement feature.

There are several obvious expansions to the present work. Experimentally, the x-ray resolution must be increased to allow for separation of the K_α and K_β decay channels. Also, improved statistics are necessary if the small effects observed are to be analyzed more rigorously. It would also be very interesting to look at other systems and see if the generalities proposed above actually exist. This remains to be done for the Ar^{q+} data we have cited throughout the present work, since the calculation of only the (microscopic) sticking probabilities for $q=3$ proved tractable. We are currently engaged in such extensions. Theoretically, it would be of great interest to pursue some of the ideas outlined above. In particular a study of participator Auger rates as core charge increases, and how these processes compete with the radiative and the core-Auger decay.

ACKNOWLEDGMENTS

We thank Ercan Alp and Dennis Brown for use of their APD detector. This work was supported by the National Science Foundation at the University of Tennessee. We are grateful to the staff of the Basic Energy Sciences Synchrotron Radiation Center at the Advanced Photon Source for their assistance in performing the experiments. The Argonne group was supported by the Chemical Sciences, Geosciences, and Biosciences Division of the Office of Basic Energy Sciences, Office of Science, U. S. Department of Energy, under Contract No. W-31-109-ENG-38. Use of the Advanced Photon Source was supported by the U. S. Department of Energy, Basic Energy Sciences, Office of Science, under Contract No. W-31-109-ENG-38.

[1] B. Crasemann, Comments At. Mol. Phys. **22**, 163 (1989).
[2] J. Tullki, G.B. Armen, T. Åberg, B. Crasemann, and M.H. Chen, Z. Phys. D: At., Mol. Clusters **5**, 241 (1987).
[3] T. Aberg and J. Tulkki, in *Atomic Inner-Shell Physics*, edited by B. Crasemann (Plenum, New York, 1985), p. 419.
[4] G.B. Armen, H. Aksela, T. Åberg, and S. Aksela, J. Phys. B **33**, R49 (2000).
[5] J.C. Levin, C. Biedermann, N. Keller, L. Liljeby, C.-S.O.R.T. Short, I.A. Sellin, and D.W. Lindle, Phys. Rev. Lett. **65**, 988 (1990).
[6] U. Alkemper, J. Doppelfeld, and F. von Busch, Phys. Rev. A **56**, 2741 (1997).

[7] T. Hayaishi, T. Tanaka, H. Yoshii, E. Murakami, E. Shigemasa, A. Yagishita, F. Koike, and Y. Morioka, J. Phys. B **32**, 1507 (1999).
[8] S. Baier, G. Gottschalk, T. Kerkau, T. Luhmann, M. Martins, M. Richter, G. Snell, and P. Zimmermann, Phys. Rev. Lett. **72**, 2847 (1994).
[9] G.B. Armen, J.C. Levin, and I.A. Sellin, Phys. Rev. A **53**, 772 (1996).
[10] We employ the bracket notation [ ] to denote holes in otherwise filled atomic subshells.
[11] V. Schmidt, *Electron Spectrometry of Atoms using Synchrotron Radiation* (Cambridge Press, Cambridge, 1997), pp. 266–267.
[12] M.A. Beno, M. Engbretson, G. Jennings, G.S. Knapp, J. Linton, C. Kurtz, U. Rütt, and P.A. Montano, Nucl. Instrum. Methods Phys. Res. A **467**, 699 (2001).
[13] M. Breinig, M.H. Chen, G.E. Ice, F. Parente, B. Crasemann, and G.S. Brown, Phys. Rev. A **22**, 520 (1980).
[14] J.B. Hastings and V.O. Kostroun, Nucl. Instrum. Methods Phys. Res. **208**, 815 (1983).
[15] S.J. Schaphorst, A.F. Kodre, J. Ruscheinski, B. Crasemann, T. Åberg, J. Tulkki, M.H. Chen, Y. Azuma, and G.S. Brown, Phys. Rev. A **47**, 1953 (1993).
[16] M.O. Krause and J.H. Oliver, J. Phys. Chem. Ref. Data **8**, 329 (1979).
[17] M.H. Chen, B. Crasemann, and H. Mark, Phys. Rev. A **21**, 436 (1980).
[18] T.A. Carlson, W.E. Hunt, and M.O. Krause, Phys. Rev. **151**, 41 (1966).
[19] A.G. Kochur, V.L. Sukhorukov, A.I. Dudenko, and Ph. V. Demekhin, J. Phys. B **28**, 387 (1995).
[20] A. El-Shemi, Y. Lofty, and G. Zschornack, J. Phys. B **30**, 237 (1997).
[21] G.B. Armen and F.P. Larkins, J. Phys. B **25**, 931 (1992).
[22] M. Meyer, E.v. Raven, B. Sonntag, and J.E. Hansen, Phys. Rev. A **43**, 177 (1991).
[23] J.A. de Gouw, J. van Eck, A.C. Peters, J. van der Weg, and H.G.M. Heideman, J. Phys. B **28**, 2127 (1995).
[24] E. Kukk, H. Aksela, A. Kivimäki, J. Jauhiainen, E. Nõmmiste, and S. Aksela, Phys. Rev. A **56**, 1481 (1997).
[25] Y. Lu, W.C. Stolte, and J.A.R. Samson, Phys. Rev. A **58**, 2828 (1998).
[26] S.B. Whitfield, C.D. Caldwell, and M.O. Krause, Phys. Rev. A **43**, 2338 (1991).
[27] J.M. Bizau, P. Gérard, F.J. Wuilleumier, and G. Wendin, Phys. Rev. A **36**, 1220 (1987).
[28] S.B. Whitfield, J. Tulkki, and T. Åberg, Phys. Rev. A **44**, R6983 (1991).
[29] G.B. Armen, J. Phys. B **29**, 677 (1996).
[30] G.B. Armen and F.P. Larkins, J. Phys. B **24**, 741 (1991).